Research Article

Detection and differentiation of paediatric renal tumours using diffusion-weighted imaging: an explorative retrospective study.

Isabel Platzer[1], Mengxia Li[2], Beate Winkler[3], Philipp Schweinfurth[4], Thomas Pabst[1], Thorsten Bley[1], Henning Neubauer[1*]

[1]Department of Diagnostic and Interventional Radiology; [2]Department of Radiation Oncology; [3]Department of Paediatrics; [4]Department of Urology; University Hospital Wuerzburg, 97080 Wuerzburg, Germany.

Abstract

Background: Diffusion-weighted imaging (DWI) is a promising supplemental technique in oncological magnetic resonance imaging (MRI). We investigated the diagnostic utility of DWI for detection and characterisation of paediatric renal tumours.

Patients and Methods: Eleven consecutive patients (median 4 years, range 4 days to 15 years, females n=9) with histologically proven renal tumours (nephroblastoma n=6, nephroblastomatosis n=2, connatal nephroblastic nephroma n=1, renal cell carcinoma n=1, local recurrence of nephroblastoma n=1) underwent routine clinical MRI at 1.5 Tesla using a standardised oncological scan including free-breathing DWI. We retrospectively analysed lesion detectability and conspicuity of tumour vs. adjacent tissue on DWI and ce-T1w.

Results: All tumour manifestations were detectable on DWI by high signal at high b-values. Mean ADC values ranged between 0.56 to 0.95 with a wide overlap between malignant lesions and nephroblastomatosis. Mean SI ratios were significantly higher on DWI, compared to ce-T1w (4.5±3.8 vs. 1.6±0.7, $p<0.001$). Six small foci of nephroblastomatosis were occult on ce-T1w imaging, but clearly delineated on DWI. One small bone metastasis was seen on DWI only. In two patients with stable unilateral manifestations of nephroblastomatosis, follow-up MRI showed mean ADC values of 1.0 ± 0.3 over three years.

Conclusion: According to our preliminary experience, DWI reliably detects paediatric renal tumours and metastases. Apparently, DWI cannot distinguish between malignant and non-malignant paediatric renal tumour entities based on mean ADC, but yields superior lesion conspicuity. DWI in free-breathing technique without the need of i.v. contrast application deserves further evaluation as stand-alone imaging, especially for follow-up in young patients.

Keywords: MRI; diffusion-weighted; renal tumour; paediatric

Introduction

Renal tumours are among the most prevalent malignancies in childhood and account for approximately 7% of all paediatric cancers (1-4). Nephroblastoma, or Wilms tumour (WT), is the most common renal tumour entity with a frequency approaching 90%. Modern treatment achieves excellent long-term survival rates (1, 2). Other renal malignancies include clear cell sarcoma (3-4%),

* **Corresponding author**: Henning Neubauer, MD, MBA. Department of Radiology, University Hospital Wuerzburg, Oberduerrbacher Str. 6, 97080 Wuerzburg, Germany. Phone: 0049-931-201-34715. Email: neubauer_h@ukw.de; inu75@web.de
Citation: Isabel Platzer, et al. Detection and differentiation of paediatric renal tumours using diffusion-weighted imaging: an explorative retrospective study. Cancer Research Frontiers. 2015 Apr; 1(2): 178-190. doi: 10.17980/2015.178

Competing Interests: The authors declare that they have no competing interests.
Received January 29, 2015; Revised April 28, 2015; Accepted May 2, 2015.

rhabdoid tumour (2%) and miscellaneous rare tumours (2%) (5). Nephroblastomatosis (NBS) represents persisting metanephric blastema, or nephrogenic rests, and is considered a premalignant lesion with a low rate of malignant transformation. NBS is seen in one-third of patients with WT and is regularly present in patients with bilateral WT, yet only few of these lesions progress to WT (6, 7). Considering this close association and co-existence of malignant and pre-malignant disease, diagnostic accuracy of imaging studies for detection and characterisation of renal lesions has an immediate impact on therapeutic decision-making, therapy monitoring and, possibly, patient outcome (8-11). Standard MRI scans with contrast-enhanced imaging reliably visualise renal tumour manifestations in children and show diagnostic performance superior to ultrasonography for detection of small foci (9). However, differentiation between tumour entities, and particularly between WT and NBS, based on MR imaging criteria alone leaves a considerable degree of uncertainty in some patients, thus prompting biopsy (12).

Diffusion-weighted MR imaging (DWI) visualises the varying degree of restriction in Brownian diffusion which water molecules are subject to in biological tissues (13). The apparent diffusion coefficient (ADC) is a quantitative measure of diffusivity in vivo. Low ADC indicating restricted diffusion is seen in cytotoxic cerebral oedema (14), in tumours with high cellularity (15) and in abscess (16). Recent studies on DWI suggest a diagnostic utility of ADC for differentiation of malignant and benign disease, and even of histological subtypes, in adult patients with renal tumours (17-20). In paediatric populations, ADC-based prediction of tumour dignity has been attempted with some success (21-23), yet there is a paucity of data on diffusion-weighted MRI of paediatric renal neoplasia. In our study, we therefore investigated the diagnostic performance of DWI for detection and differentiation of paediatric renal tumours.

Patients and methods

At our institution, extracranial DWI has been part of routine clinical scanning since 2008 and has been integrated into routine paediatric magnetic resonance imaging (MRI) protocols for more than five years. For this study, we retrospectively evaluated consecutive paediatric patients with renal tumours. The study population includes eleven consecutive patients (nine females) with a mean age of 4.8 ± 4.0 years (median four years, range 4 days to 15 years) at initial diagnosis who were examined between 2009 and 2014. Another two patients did not have DWI at initial staging for technical reasons and were excluded from this study. All patients were treated at the Department of Paediatrics of our institution and were referred to routine oncological MRI due to clinically and/or sonographically suspected renal mass. All study work was conducted in accordance with the Helsinki Declaration. Retrospective analysis of anonymized data from routine examinations for scientific purposes is covered by the treatment contract between patients and our university hospital. Informed written consent was obtained from the legal guardians of all patients for all diagnostic and therapeutic measures. Surgical and histopathological correlation was available for all patients.

All routine MRI examinations were performed according to our oncological standard imaging protocol at 1.5 Tesla (Magnetom Symphony, Magnetom Avanto, Magnetom Aera; Siemens Healthcare, Erlangen, Germany). Seven patients (age range 2 days to 6 years) were sedated and monitored by a paediatric anaesthesiologist. All patients were scanned in supine position with multi-channel phased-array body coils and an i.v. line in place. The scan protocol comprised T2-weighted (T2w) turbo spin-echo (TSE), pre-contrast and contrast-enhanced fat-saturated T1-weighted (ce-T1w) sequences. Prior to i.v. contrast administration, DWI was acquired as transverse (axial) single-shot diffusion-weighted echo-planar imaging (SS-DW-EPI) with diffusion-sensitizing gradients (b-values of 50 and 800 s/mm2) applied sequentially along the three orthogonal directions. Typical scan parameters were repetition time (TR) 9000 ms, echo time (TE) 126 ms, 8 averages, epi factor 128, trace-weighted, spectral fat saturation, slice thickness 4-6 mm, base resolution 128, inplane resolution 1.8x1.8 mm2, acquisition time 5 minutes. All DWI scans were performed in standard free-breathing acquisition without triggering or motion correction techniques. Contrast-enhanced fat-saturated T1w images obtained as transverse 2D- fast low angle shot (FLASH) (typical parameters: TR 86 ms, TE 3.8 ms, flip angle 90°, field of view (FOV) 250 mm, in-plane resolution 1.3 mm x 1.3 mm, slice thickness 4-6 mm, spectral fat saturation, breath-holding) or, in sedated patients, as transverse T1w TSE (typical parameters: TR 2000 ms, TE 2.5 ms, flip angle 15°, FOV 350 mm, in-plane resolution 0.7 mm x 0.7 mm, slice thickness 4 mm, spectral fat saturation) with respiratory triggering.

Image analysis for detection and visual tissue

Table 1. Tumour size, signal intensity ratios on contrast-enhanced T1w and DWI, ADC values (unit: 10−3mm2/s) of tumorous lesions and ADC values of reference tissues. All patients with Wilms tumour underwent neoadjuvant chemotherapie, followed by a pre-operative staging MRI ("post-therapy") and surgical treatment.

	Wilms tumour pre-therapy	Wilms tumour post-therapy	Wilms tumour metastases	all malignancies pre-therapy	NBS
number of patients/lesions	6/6	6/6	3/6	9/14	5/17
mean size (range), cm	8.4 (2.6 ... 10)	4.1 (2 ...6.3)	4.8 (1 ... 11)	6.5 (1 ... 13)	1.0 (0.3 ... 2.5)
SI ratio ce-T1w	1.6 ± 0.2	1.4 ± 0.2	2.3 ± 0.9	1.9 ± 0.8	1.3 ± 0.8
SI ratio DWI	3.3 ± 0.1	2.8 ± 1.1	10.1 ± 4.9	6.5 ± 4.2	2.3 ± 1.8
ADC tumour, small ROI	0.6 ± 0.1	0.9 ± 0.4	-	0.7± 0.3	-
ADC tumour, large ROI	1.0 ± 0.4	1.5 ± 0.4	0.8 ± 0.4	1.0 ± 0.4	0.7 ± 0.3
ADC muscle	1.1 ± 0.1	1.2 ± 0.2	1.2 ± 0.1	1.2 ± 0.2	1.2 ± 0.1
ADC renal cortex	1.7 ± 0.2	1.7 ± 0.2	1.6 ± 0.2	1.7 ± 0.2	1.6 ± 0.2

ADC = apparent diffusion coefficient (unit: 10−3mm2/s) , NBS = nephroblastomatosis, SI = signal intensity ratio;

characterisation of tumour lesions was conducted as a blinded consensus reading of two experienced observers: The first reader was a resident with five years training in radiology and with special training in paediatric imaging (I. P.) and the other a board-certified paediatric radiologist with seven years of experience in extra-cranial DWI (H. N.). The readings of DWI and ce-T1w imaging were performed one week apart to avoid recall bias to the extent possible in our small group of patients. Diffusion-weighted (DW) images were read in default window settings and always assessed in combination with the ADC map so as to prevent false-positive readings originating a from "T2 shine-through" artefact. T2 shine-through originates from the strong T2w signal of fluids and is characterised by a persisting high signal at high b values in combination with high ADC. Lesions showing high signal on DW images both at low and at high b-value with a corresponding low measurement on the ADC map were considered as exhibiting restricted diffusion. Cystic portions of the tumour were assumed in areas of high signal at low b-value, low signal at high b-value and corresponding high ADC (Figure 1). We then measured signal intensity of renal tumour foci and, if present, of extra-renal metastases manually with region of interest (ROI) technique. Signal intensity ratios of tumour vs. adjacent tissue were calculated for ce-T1w and DWI. Mean ADC was measured on automatically computed ADC maps with a large circular ROI comprising the whole of the tumorous lesion on one representative transversal section. In large and heterogeneous tumours (i.e., WT and renal cell carcinoma), we performed an additional small ROI measurement with a ROI size of 1 to 2 cm2 in the portion of the tumour with the highest degree of restricted diffusion, thus omitting inhomogeneous or cystic areas (Figure 1). In addition, mean ADC of the renal cortex and the erector spinae muscles were measured as reference. All image analyses were performed off-line on a Syngo Plaza workstation (Siemens Healthcare, Erlangen, Germany).

Statistical analysis

Normally distributed data is presented as mean ± standard deviation. The comparison of signal intensity ratios between ce-T1 and DWI was performed with a two-sided Wilcoxon signed ranks test. $\alpha < 0.05$ was considered as indicating statistical significance. Spreadsheet analyses were performed with Microsoft Excel 2007 for Windows. Statistical tests were calculated with IBM SPSS 21 for Windows.

Results

The eleven patients in our study group were diagnosed with nephroblastoma (WT) n=6, nephroblastomatosis (NBS) n=2, connatal mesoblastic nephroma (CMN) n=1, juvenile renal cell carcinoma (RCC) n=1 and local recurrence of nephroblastoma n=1. All MRI studies yielded diagnostic image quality, and all tumour lesions identified on standard MRI sequences were detected on DWI, as well. Data on imaging characteristics and quantitative measurements are summarised in Table 1. Measured with small ROI technique, all tumour lesions except for two small NBS foci had low mean ADC values < 1.0. Neither ADC nor SI ratios on DWI or ce-T1w imaging differed significantly between malignant disease and NBS. Patients with WT, with WT recurrence and with RCC all showed inhomogeneous tumour signal and signal elevations on T2w, equivalent to cystic portions, in at least a small part of the tumour. Solid portions of these lesions exhibited varying degrees of markedly restricted diffusivity and hypointense signal on ce-T1w indicating hypoperfusion, as compared to normal renal cortex. All NBS foci and the CMN were characterised by homogenous signal, markedly hyperintense on DWI, moderately hyperintense on T2w and hypointense on ce-T1w.

Patients with primary diagnosis of Wilms tumour

All six patients with newly diagnosed WT underwent MR scanning before and after neoadjuvant standard chemotherapy (SIOP 2001 (24)). In two of these patients, WT was the only tumour focus on initial staging. The third WT patient had multiple retroperitoneal and liver metastases at primary diagnosis (Figure 2). Another patient had three ipsilateral foci of NBS measuring 15 to 26 mm and three small contralateral NBS lesions of 3 to 5 mm in diameter (Figure 3 and 4). Of these, the three small NBS foci were virtually occult on contrast-enhanced T1w imaging, but showed high signal intensity on DWI, whereas the ipsilateral larger NBS foci were detectable on both DWI and ce-T1w. The fifth patient had bifocal WT in one kidney and additional multiple small bilateral foci of nephroblastomatosis. Of the latter, five lesions measuring 5 to 10 mm in diameter were visible both on DWI and ce-T1w, while several

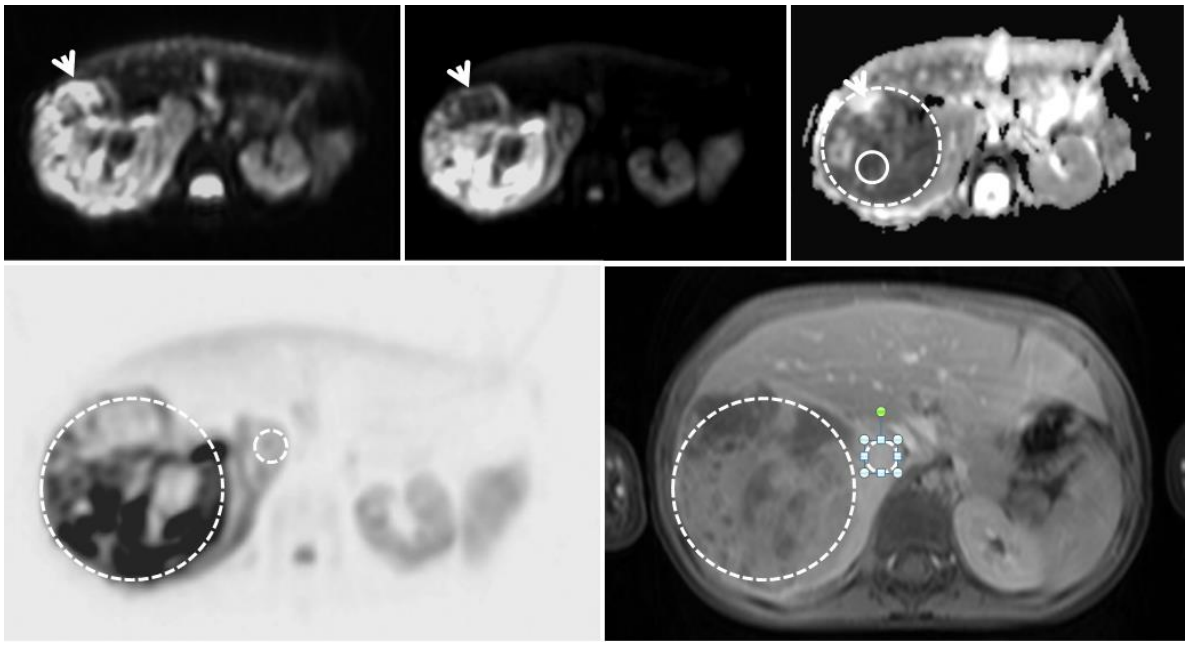

Figure 1. Three-year-old girl with primary diagnosis of Wilms tumour of the right kidney. Diffusion-weighted MRI (1.5 Tesla Magnetom Symphony) shows cystic portions within the heterogeneous lesion (arrowheads) with high signal on DWI b=50 (upper row, left), low signal on DWI b=800 (upper row, middle) and high mean ADC of 2.6 (upper row, right). ADC of the tumor was measured as 1.28 with large ROI (upper row, right, dotted line) and as 0.55 with small ROI (solid line). Signal intensity ratios were measured with ROIs on DWI b=800 (lower row, left, inverted grey scale) and on contrast-enhanced T1w images (lower row, right, respiratory-triggered T1 TSE FS) as signal intensity of the tumour versus signal intensity of adjacent normal renal tissue.

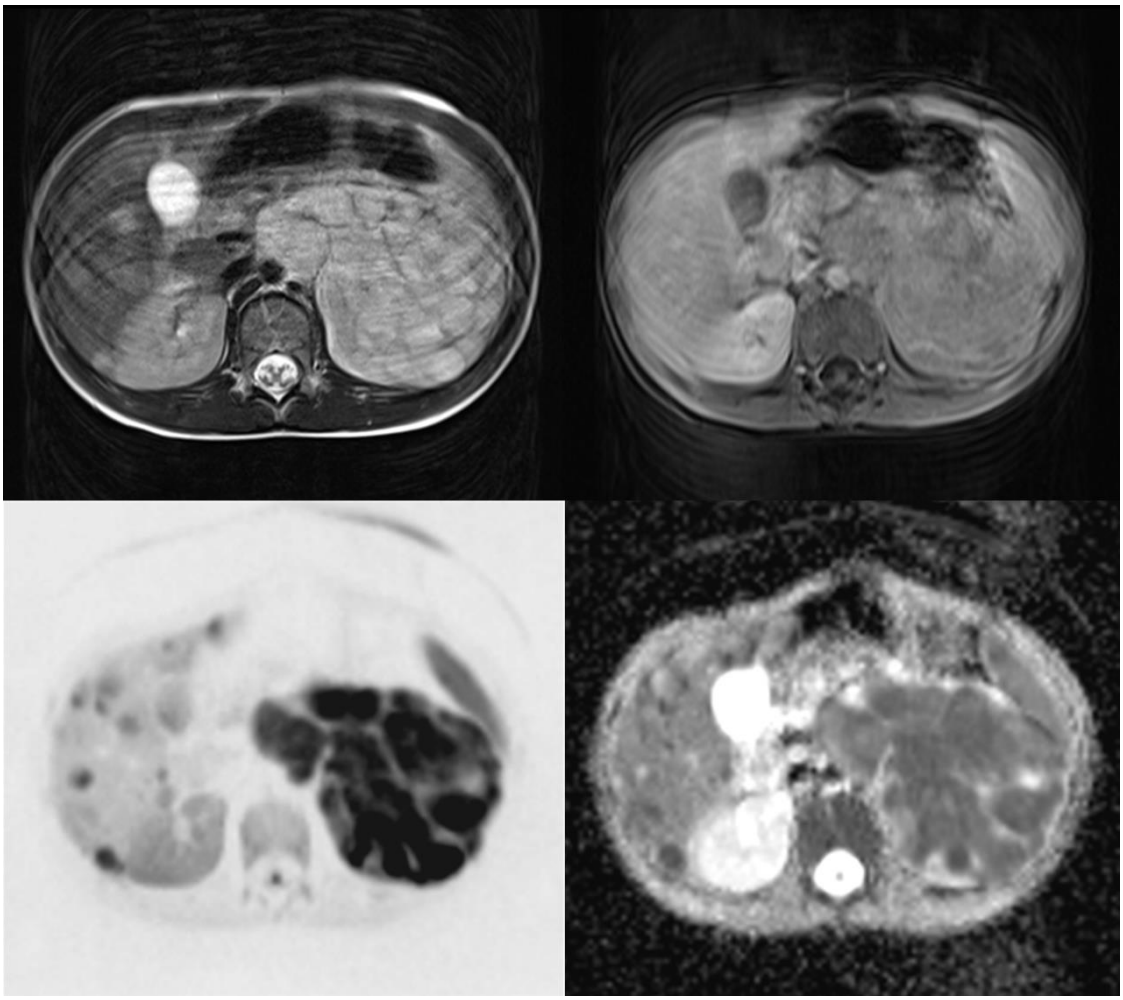

Figure 2. Seven-year-old boy with primary diagnosis of Wilms tumor of the left kidney. The boy came to the emergency room in bad clinical condition. Ultrasonography showed a large mass in the left upper abdomen, and the child was referred to emergency MRI. Image quality of standard sequences (upper left: T2w TSE, upper right: ce-T1w FLASH with fat saturation) was degraded, as the patient could not well cooperate with breathholding and respiratory triggering. Free-breathing DWI (lower left: DWI b=800, inverted grey scale) clearly delineates the large inhomogenous renal tumour as well as multiple liver metastases with superior lesion conspicuity. The patient also had retroperitoneal lymphonodal metastases (not shown). The lesions exhibit markedly restricted diffusivity represented in dark shade on the inverted DWI image (lower left) and in corresponding darkish-grey shades on the ADC map (lower right).

smaller foci would have been missed on ce-T1w alone.

Finally, one WT patient presented with a 5 mm nephrogenic rest in the contralateral kidney visible on both contrast-enhanced and diffusion-weighted sequences. Involvement of the renal vein was not observed. Mean signal intensity ratio of WT was significantly higher on DWI, compared to ce-T1w ($p=0.043$).

All patients underwent neoadjuvant chemotherapy and pre-operative MRI re-staging, which confirmed a marked reduction in tumour size, a decrease in signal intensity ratios for both ce-T1w and DWI and an increase in mean ADC as indicators of response to treatment in all patients (Table 1). After successful treatment with surgical tumour resection and complete remission, five patients remained in complete remission at a median follow-up of 29 months, while one patient suffered progressive disease with new pleural metastases nine months after initial diagnosis.

Patients with other renal malignancies

One patient with a history of left-sided Wilms tumour and resection of retroperitoneal, pancreatic and small-bowel metastases was newly diagnosed with a large local tumour recurrence and an intrapelvic metastasis. A small vertebral bone metastasis in this patient was visible on DWI only. Chemotherapy did not induce any significant response in terms of tumour size (pre- vs. post-therapy tumour diameter constant at 60 mm), i.v. contrast uptake or mean ADC (pre- vs. post-therapy ADC: 0.73 vs. 0.86).

A 15-year-old girl without clinical signs or history of Hippel-Lindau syndrome had a large solitary tumour which showed all imaging characteristics of WT including heterogeneous signal on standard sequences and DWI. The unusually late manifestation of presumed WT and differential diagnoses were discussed with the patient's parents and in the interdisciplinary tumour conference. Based on consensus, the girl underwent standard neoadjuvant treatment for WT (SIOP 2001). Preoperative MRI re-staging revealed constant tumour size (12 mm) and persistingly low ADC values in the solid portions of the tumour (pre- vs. post-therapy ADC: 0.54 vs. 0.65). Histopathological work-up of the resected lesion proved juvenile renal cell carcinoma with little response to neoadjuvant chemotherapy and tumour necrosis in < 5%.

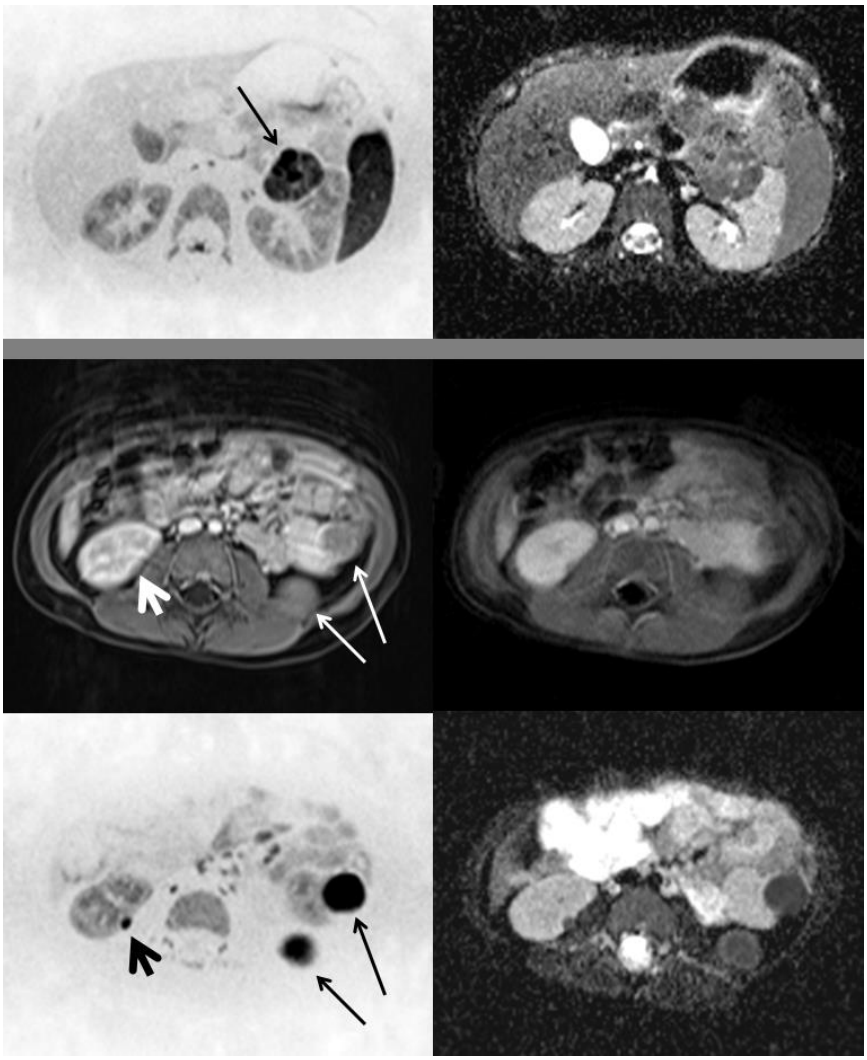

Figure 3.Three-year-old girl with a 2,6 cm left-sided Wilms tumor (arrow, upper row left: DWI b=800, inverted grey scale, upper row right: ADC map). In the caudal renal parenchyma, additional bilateral lesions were vaguely visible on contrast-enhanced imaging (middle row left: T1w VIBE, middle row right: T1 TSE water excitation with respiratory triggering), but were confirmed as foci of highly restricted diffusivity on DWI (lower row left: DWI b=800, inverted grey scale, lower row right: ADC map). Free-breathing DWI showed virtually no motion artefacts and clearly visualised even the 5 mm right-sided lesion.

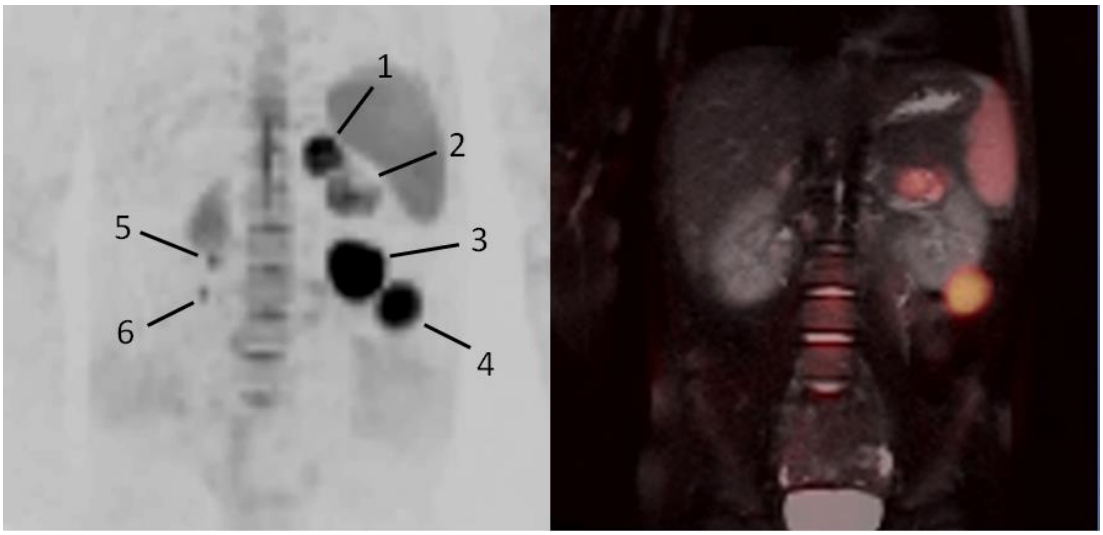

Figure 4. Same patient as in Figure 3. An additional coronal DWI scan (left image: coronal DWI b=800, inverted grey scale, maximum intensity projection (MIP) - reconstruction) was performed to improve visualisation of the multiple renal lesions. The patient was eventually diagnosed with Wilms tumor (lesion 2) and three large foci of NBS (lesions 1, 3 and 4) in the left kidney, which were all histologically confirmed after neoadjuvant chemotherapy and left-sided nephrectomy. Three small foci (3-5 mm) in the left kidney (lesions 5 and 6, lesion 7 not visible on MIP reconstruction) assumed to present additional manifestations of NBS were no longer visible after neoadjuvant treatment and did not relaps during two years of follow-up. Overlay of colourised DWI signal on standard sequenzes (right image: colourised coronal DWI b=800 overlay on coronal T2w HASTE, 3D FUSION, Siemens Medical) facilitates co-registration of DWI signal and anatomical background and is useful in communicating MRI findings to referring physicians.

Routine abdominal ultrasonography discovered a renal tumour with 2.5 cm in diameter in a 4-days-old girl. The very young patient age and the relatively large solitary lesion were suggestive of CMN. Histopathology after tumour resection confirmed this diagnosis. The MRI signal of the lesion mimicked NBS with homogeneous hypointense signal on ce-T1w and marked homogenous diffusion restriction throughout the tumour.

Patients with nephroblastomatosis/nephrogenic rests

Three of our WT patients (50%) had additional foci of NBS or nephrogenic rests in the ipsilateral and/or contralateral kidney. Ipsilateral foci were larger with a diameter up to 2.5 cm, while none of the contralateral lesions exceeded 5 mm. Two young patients with NBS and a history of nephron-sparing resection of extensive NBS have been followed up at our institution with ultrasonography and MRI follow-up for 3 years and 6 years (Figure 5). Each had one small 5 mm NBS remnant which was found constant in the long run in terms of lesion size and signal.

All NBS manifestations showed slightly hypointense homogeneous signal on ce-T1w, compared to the renal cortex. Subjective lesion conspicuity was superior on DWI for all NBS lesions, and SI ratios on DWI were higher, compared to ce-T1w ($p<0.05$, Wilcoxon signed rank test) (Table1). Of the 17 NBS lesions quantified for our study, 11 (65%) were detectable with both ce-T1w and DWI, all of these measuring 5 mm or above in diameter, while six NBS foci would have been missed without DWI. These small lesions were virtually occult on ce-T1w, but all showed high signal on DWI at high b-values. The large NBS foci had mean ADC values ranging between 0.3 and 0.5, while the small lesions with 3 to 5 mm in diameter were measured with higher mean ADC of 0.7 to 1.2. Mean ADC of NBS was 0.7 ± 0.3 (Table 1).

Discussion

Our explorative single-centre study with retrospective data analysis demonstrates the usefulness of DWI for detection of renal tumours and their metastases in paediatric patients. All tumour

lesions detectable on standard MRI were also seen on DWI, but were displayed with significantly higher signal on diffusion-weighted images and thus stood out from the adjacent anatomical structures. A number of small NBS foci with low signal intensity ratios on ce-T1w were identified with certainty only after correlation with the diffusion-weighted images. DWI also detects additional NBS lesions. The preliminary experience from our study data, however, suggests that DWI cannot differentiate between malignant renal tumours and NBS/nephrogenic rests, based on mean ADC values.

Renal tumours account for a small, but significant proportion of malignancies in children (1). Wilms tumour (WT), the most prevalent entity by far, is highly responsive to modern multi-modal therapy, and a majority of WT patients enjoys excellent long-term survival rates (25). According to European guidelines, therapeutic standard in WT patients is initial diagnostic imaging for tumour staging, neoadjuvant chemotherapy, re-staging and tumour nephrectomy, possibly followed by post-operative chemotherapy and irradiation depending on tumour stage. Pre-therapeutic tumour biopsy is not usually performed in young children presenting with solid renal tumours and imaging findings consistent with WT (5). Standard MR imaging, however, cannot reliably differentiate between the various renal tumour entities, nor confidently predict malignancy or the biological potential of a renal mass (26). Furthermore, considering the presence of bilateral WT in about 10% of the patients (27), the frequent association of WT and nephrogenic rests or nephroblastomatosis (NBS) (6-7) and the low rate of malignant transformation of NBS lesions (6-8), therapy planning and options for nephron-sparing surgery would certainly benefit from more accurate image-based characterisation of these renal lesions. In patients with bilateral WT undergoing nephron-sparing surgery (11), accurate detection and description of additional NBS foci may help to optimize surgical resection and may result in higher proportions of preserved renal tissue.

DWI is a MR imaging technique that visualises the degree of restriction experienced by water molecules in the extracellular space of biological tissues. The DWI signal is closely related to tissue cellularity (15), among other factors, and previous studies found evidence for improved tissue characterisation with quantitative measures of diffusivity. In paediatric oncology, embryonal malignant tumours typically present with high cellularity, characterized by

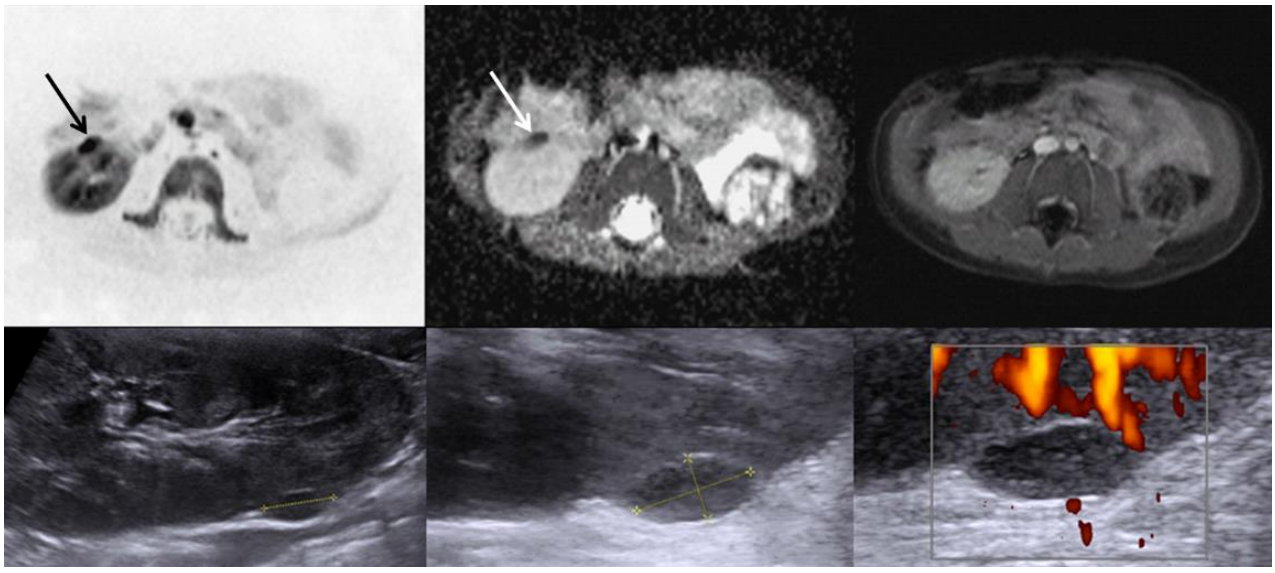

Figure 5. Four-year-old girl with a history of left-sided nephrectomy and right-sided nephron-sparing surgery for bilateral extensive NBS. Several post-operative ultrasound follow-up examinations of the right kidney had not revealed remnant or recurrent disease. Diffusion-weighted MRI showed a small focus of restricted diffusion (arrow, upper row, left, DWI b=800, inverted grey scale) and corresponding low ADC (arrow, upper row, middle, ADC map), while no focal lesion was visible on ce-T1w (upper row, right, T1 TSE FS with respiratory trigger). Targeted ultrasound then depicted the hypoechogenic and hypovascularised 5 mm lesion (lower row, left: B-mode ultrasound, middle: magnification and calipers, right: power doppler) consistent with remaining NBS. To date, the lesion has been found constant over three years of ultrasonographic and MRI follow-up.

densely packed cells and consecutively narrowed extra-cellular space with many barriers to the diffusion of extracellular water. In contrast, benign tumours or lesions rich in interstitial stroma are characterized by a low cell count, wider extracellular space and therefore less impeded diffusion (15). While DWI features of renal tumours in adults have been a focus of several recent studies and a meta-analysis (18-20), there is a paucity of such data from paediatric cohorts. Tumour characterisation, based on ADC, has been reported in other paediatric tumour entities. DWI was able to differentiate between neuroblastoma and ganglioneuroblastoma/ganglioneuroma (21) and between malignant and non-malignant osseous and soft-tissue lesions (23). Cut-off ADC values around 1 × 10−3mm2/s with lower ADC being predictive of malignancy were found in these studies (21, 23). Inflammatory musculoskeletal lesions, on the other hand, showed markedly elevated ADC values ranging from 1.4 to 2.6 × 10−3mm2/s (28) without overlap to musculoskeletal malignancies (23).

In our present study, free-breathing DWI produced high-quality scans of our paediatric patients (Figure 2) and showed high sensitivity for renal tumour foci. In our small study group, we found evidence that allows us to extent the concept of DWI-based tumour detection to paediatric renal masses. Mean signal intensity of tumour foci, as compared to adjacent tissue, was higher on DW images than on contrast-enhanced images, which translates into higher lesion contrast. We decided to use signal intensity ratios as the quantitative metric in our study, rather than contrast-to-noise ratio (CNR). Using modern scanner hardware and software, image noise is no longer evenly distributed in MR images acquired with multi-channel receiver coils and built-in image filtering. The traditional straight-forward approach of measuring image noise with ROIs on the images may be affected in an unpredictable manner and extent under such circumstances. Quantification of image noise and evaluation of noise distribution by the means of field maps was not performed in our clinical setting.

Although DWI allowed ready tumour detection in all our patients, we could not, however, differentiate malignant from non-malignant renal tumours based on ADC. Mean ADC values lower than 1.0 were seen in all malignant lesions, but also in NBS, with the small ROI technique. In heterogeneous tumours containing both solid and cystic tissue, it is our practical approach to target portions of the tumour exhibiting restricted diffusion and to measure ADC with a small ROI of approximately 1 to 2 cm2 there. In contrast to previous experience with other paediatric tumour entities (29) and with renal tumours in adult patients (20), however, non-malignant lesions in our study, namely the nephrogenic rests and NBS foci, also showed markedly restricted diffusivity and mean ADC less than 1 × 10−3mm2/s. Reference ADC values measured in the renal cortex and in the erector spinae muscle showed little variation between patients or between MRI scanners and showed no substantial across-study variation in comparison to previously reported data (23, 30). The association of relatively high ADC in small NBS lesions and low ADC in larger NBS lesions is very likely the result of partial volume effects, as the size of these small NBS foci (3-5 mm) approached the in-plane resolution (1.8 mm2) of our DWI scan. High ADC of the surrounding renal cortex may thus explain a higher ADC in small NBS lesions, compared to large foci of NBS.

On both DWI and on standard MRI in our study, NCC and CMN, both representing rare renal tumour entities, mimicked WT and NBS, respectively. Heterogeneity and cystic tumour portions were the only imaging findings relatively characteristic of WT, as compared to NBS, and were observed on both DWI and ce-T1w imaging. Although data from larger patient cohorts is certainly needed, it presently appears unlikely that DWI will provide information that allows accurate characterisation of WT, NBS and other paediatric renal masses based on ADC quantification with mono-exponential modelling alone. A new promising DWI technique is intra-voxel incoherent motion (IVIM) technique (31) which distinguishes between diffusion and perfusion effects both contributing to the DWI signal and was found useful to discriminate renal tumour subtypes in adult patients (32). Other DWI-based methods recently under investigation are the diffusion kurtosis model (33, 34) and "Vascular, Extracellular and Restricted Diffusion for Cytometry in Tumors" (VERDICT) - MRI, the latter combining DWI with a complex mathematical model of tumour tissue and taking into account factors such as cell size, vascular volume fraction, intra- and extracellular volume fractions, and pseudo-diffusivity associated with blood flow (35).

Earlier studies investigating DWI of tumours undergoing chemotherapy reported markedly increasing diffusivity in responsive malignant tumours, supposedly as a result of tumour necrosis, reduced cellularity and concomitant tissue oedema

(36). All the Wilms tumour manifestations in our study that were responsive to chemotherapy were likewise seen with a marked increase in ADC and a substantial reduction in tumour size on the pre-operative re-staging (Table 1), while the two non-responsive lesions, that is the juvenile NCC and the local WT recurrence, had persisting low mean ADC. Based on our preliminary experience, ADC quantification may therefore be a useful supplemental technique for evaluating response to therapy in children undergoing neoadjuvant treatment for Wilms tumour.

For presentation of diffusion-weighted images in print and in clinical rounds, we found it helpful to use images with an inverted grey scale, as seen in Figures 1 through 5. From our experience, this mode of presentation carries a smaller risk of degraded image reproduction in print. Furthermore, our clinicians are used to looking at scintigraphic studies and PET images. As DWI with inverted grey scale somewhat resembles bone scintigraphy or PET scans, we often use inverted DWI when communicating our findings to the referring clinicians. To date, there is no data to support the hypothesis that grey scale inversion for diffusion-weighted images may be helpful for routine readings, as it was reported for the detection of pulmonary nodules on chest films (37).

Limitations

The retrospective design of our explorative study, the limited number of patients available for analysis and the different scanner hardware used in data acquisition all need to be taken into account when drawing conclusions from the presented study data. Apart from Wilms tumour and nephroblastomatosis, other paediatric renal tumour entities are generally rare with frequencies below 5%, so that only one case of NCC and CMN each were among our study patients. In fact, only rudimentary statistical testing was possible considering the small sample size. A prospective multi-centre approach with standardised examination protocols will be necessary to recruit larger patient cohorts and to arrive at more definite conclusions. MRI examinations in our study were performed at 1.5 Tesla on three different MR scanners from the same manufacturer with very similar scanning parameters. Overall image quality was superior for examinations performed on the Avanto and Aera scanner, compared to the older Magnetom Symphony. At any rate, a potential impact of hardware and software configuration on our study results cannot completely be ruled out. A technical issue of concern is the still limited spatial resolution of DWI, relative to small-sized NBS lesions, which renders quantitative ROI analysis of ADC susceptible to partial volume effects, as discussed above.

Another limitation arises from the technical specifications chosen for the DWI sequence. We acquired DW images at two b-values only, being aware that bi-exponential modelling based on three or more b-values produces more accurate ADC values (13). While ADC values computed from a bi-exponential model may differ to some extent from the ADC values reported in our study, the differences would be small, in our experience, compared to variability arising from intra- and inter-observer variability of ADC measurements in a clinical setting. Time is a crucial factor in paediatric MRI and measuring additional b-values considerably adds to total scanning time. We argue that the potential benefit of measuring additional b-values or higher b-values, requiring more averages because of less signal (13), would not justify the extra-time and the additional discomfort to the patients, some seriously ill and in bad clinical condition and some undergoing MRI in sedation.

As it is, the study presents proof-of-concept work. Future studies should include inter-observer variability analyses and collect observations at different levels of experience to identify learning curves with DWI and standard MRI sequences.

Conclusions

Our study is a first systematic attempt to evaluate the diagnostic performance of diffusion-weighted imaging in paediatric patients with renal tumours. Evidently, DWI is useful for detecting and monitoring paediatric renal masses. While DWI based on ADC with mono-exponential modelling may add little diagnostic utility to standard MRI for discriminating between various renal tumour entities, lesion conspicuity on DWI was found superior to contrast-enhanced T1w imaging because of a higher inherent lesion-to-background signal and less interference of motion artefacts. Advanced DWI techniques, such as kurtosis imaging or IVIM, should be evaluated for imaging paediatric renal tumours. DWI is particularly well-suited for young patients for its merits of fast scanning in free-breathing technique without the need of breath-holding, respiratory triggering or i.v. contrast application. DWI being a gentle and truly non-invasive scanning technique deserves further evaluation as a supplement to

standard MRI protocols and as stand-alone imaging in young patients.

Acknowledgements

The authors would like to thank the MRI technicians for performing the MR scans in high quality and for taking care of the patients during the examination. No external sources of funding were used in this research.

Abbreviations

ADC	apparent diffusion coefficient;
ce-T1w	contrast-enhanced T1-weighted;
CMN	connatal mesoblastic nephroma;
DWI	diffusion-weighted imaging;
FLASH	fast low angle shot ;
FOV	field of view;
IVIM	intra-voxel incoheren motion;
NBS	nephroblastomatosis;
RCC	renal cell carcinoma;
ROI	region of interest;
SI	signal intensity;
SS-DW-EPI	single-shot diffusion-weighted echo-planar;
T1w	T1-weighted;
T2w	T2-weighted;
TE	echo time;
TR	repetition time;
TSE	turbo spin-echo;
WT	Wilms tumour

References:

1. Dome JS, Fernandez CV, Mullen EA, Kalapurakal JA, Geller JI, Huff V, et al. Children's Oncology Group's 2013 Blueprint for Research: Renal Tumors. Pediatr Blood Cancer. 2013 Jun; 60(6):994-1000. DOI: 10.1002/pbc.24419.
2. Swinson S, McHugh K. Urogenital tumours in childhood. Cancer Imaging. 2011 Oct 3;11 Spec No A:S48-64. DOI: 10.1102/1470-7330.2011.9009.
3. Howlader N, Noone AM, Krapcho M, Garshell J, Miller D, Altekruse SF, et al. (eds). SEER Cancer Statistics Review, 1975-2011, National Cancer Institute. Bethesda, MD, http:// http://seer.cancer.gov/archive/csr/1975_2011/, based on November 2013 SEER data submission, posted to the SEER web site, April 2014 (last access: April 30th, 2015).
4. Ali AN, Diaz R, Shu HK, Paulino AC, Esiashvili N. A Surveillance, Epidemiology and End Results (SEER) program comparison of adult and pediatric Wilms' tumor. Cancer. 2012 May1; 118(9):2541-51. DOI: 10.1002/cncr.26554.
5. Vujanic GM, Sandtstedt B. The pathology of Wilms' tumour (nephroblastoma): the International Society of Paediatric Oncology approach. J Clin Pathol. 2010 Feb; 63(2):102-9. DOI: 10.1136/jcp.2009.064600.
6. Perlman E, Dijoud F, Boccon-Gibod L. (Nephrogenic rests and nephroblastomatosis). Article in French. Ann Pathol. 2004 Dec; 24(6):510-5.
7. Lonergan GJ, Martinez-Leon MI, Agrons GA, Montemarano H, Suarez ES. Nephrogenic rests, nephroblastomatosis and associated lesions of the kidney. Radiographics. 1998 Jul-Aug; 18(4):947-68.
8. Owens CM, Brisse HJ, Olsen OE, Begent J, Smets AM. Bilateral disease and new trends in Wilms tumour. Pediatr Radiol. 2008 Jan; 38(1):30-9. DOI: 10.1007/s00247-007-0681-0
9. Rohrschneider WK, Weirich A, Rieden K, Darge K, Tröger J, Graf N. US, CT and MR imaging characteristics of nephroblastomatosis. Pediatr Radiol. 1998 Jun; 28(6): 435-43.
10. Millar AJ, Davidson A, Rode H, Numanoglu A, Hartley PS, Daubenton JD, et al. Bilateral Wilms' tumors: a single-center experience with 19 cases. J Pediatr Surg. 2005 Aug; 40(8): 1289-94. DOI: 10.1016/j.jpedsurg.2005.05.013
11. Millar AJ, Davidson A, Rode H, Numanoglu A, Hartley PS, Desai F. Nephron-sparing surgery for bilateral Wilms' tumours: a single-centre experience with 23 cases. Afr J Paediatr Surg. 2011 Jan-Apr; 8(1): 49-56. DOI: 10.4103/0189-6725.78669.
12. Cox SG, Kilborn T, Pillay K, Davidson A, Millar AJW. Magnetic Resonance Imaging Versus Histopathology in Wilms Tumor and Nephroblastomatosis: 3 Examples of Noncorrelation. J Pediatr Hematol Oncol. 2014 Mar; 36(2): e81-4. DOI: 10.1097/MPH.0b013e318290c60d.
13. Bammer R. Basic principles of diffusion-weighted imaging. Eur J Radiol. 2003 Mar; 45(3): 169-84. DOI: 10.1016/S0720-048X(02)00303-0
14. Schaefer PW, Grant PE, Gonzalez RG. Diffusion-weighted MR imaging of the brain. Radiology. 2000 Nov; 217(2): 331-45. DOI:

10.1148/radiology.217.2.r00nv24331
15. Humphries PD, Sebire NJ, Siegel MJ, Olsen OE. Tumors in Pediatric Patients at Diffusion-weighted MR Imaging: Apparent Diffusion Coefficient and Tumor Cellularity. Radiology. 2007 Dec; 245(3): 848-54. DOI: 10.1148/radiol.2452061535
16. Neubauer H, Platzer I, Mueller VR, Meyer T, Liese J, Koestler H, et al. Diffusion-weighted MRI of abscess formations in children and young adults. World J Pediatr. 2012 Aug; 8(3): 229-34. DOI: 10.1007/s12519-012-0362-4.
17. Razek AA, Farouk A, Mousa A, Nabil N. Role of diffusion-weighted magnetic resonance imaging in characterization of renal tumors. J Comput Assist Tomogr. 2011 May-Jun; 35(3): 332-6. DOI: 10.1097/RCT.0b013e318219fe76.
18. Kierans AS, Rusinek H, Lee A, Shaikh MB, Triolo M, Huang WC, Chandarana H. Textural differences in apparent diffusion coefficient between low- and high-stage clear cell renal cell carcinoma. AJR Am J Roentgenol. 2014 Dec; 203(6): W637-44. DOI: 10.2214/AJR.14.12570.
19. Sasamori H, Saiki M, Suyama J, Ohgiya Y, Hirose M, Gokan T. Utility of apparent diffusion coefficients in the evaluation of solid renal tumors at 3T. Magn Reson Med Sci. 2014; 13 (2): 89-95. DOI: 10.2463/mrms.2013-0038
20. Lassel EA, Rao R, Schwenke C, Schoenberg SO, Michaely HJ. Diffusion-weighted imaging of focal renal lesions: a meta-analysis. Eur Radiol. 2014 Jan; 24(1): 241-9. DOI: 10.1007/s00330-013-3004-x.
21. Gahr N, Darge K, Hahn G, Kreher BW, von Buiren M, Uhl M. Diffusion-weighted MRI for differentiation of neuroblastoma and ganglioneuroblastoma/ganglioneuroma. Eur J Radiol. 2011 Sep; 79(3): 443-6. DOI: 10.1016/j.ejrad.2010.04.005.
22. Oka K, Yakushiji T, Sato H, Fujimoto T, Hirai T, Yamashita Y, et al. Usefulness of diffusion-weighted imaging for differentiating between desmoid tumors and malignant soft tissue tumors. J Magn Reson Imaging. 2011 Jan; 33(1):189-93. DOI: 10.1002/jmri.22406.
23. Neubauer H, Evangelista L, Hassold N, Winkler B, Schlegel PG, Köstler H, et al. Musculoskeletal tumorous and tumour-like lesions: diagnostic utility of diffusion-weighted MRI for detection and differentiation in paediatric patients. World J Pediatr. 2012 Nov; 8(4): 342-9. DOI: 10.1007/s12519-012-0379-8.
24. van den Heuvel-Eibrink MM, van Tinteren H, Bergeron C, Coulomb-L'Hermine A, de Camargo B, Leuschner I, et al. Outcome of localised blastemal-type Wilms tumour patients treated according to intensified treatment in the SIOP WT 2001 protocol, a report of the SIOP Renal Tumour Study Group (SIOP-RTSG). Eur J Cancer. 2015 Mar; 51(4): 498-506. DOI: 10.1016/j.ejca.2014.12.011.
25. Pritchard-Jones K. Controversies and advances in management of Wilms tumour. Arch Dis Child. 2002 Sep; 87(3): 241-4.
26. Lowe LH, Isuani BH, Heller RM, Stein SM, Johnson JE, Navarro OM, et al. Pediatric renal masses: Wilms tumor and beyond. Radiographics. 2000 Nov-Dec; 20(6): 1585-603.
27. Petruzzi MJ, Green DM. Wilms tumour. Pediatr Clin North Am. 1997 Aug; 44(4): 939-52.
28. Neubauer H, Evangelista L, Morbach H, Girschick H, Prelog M, Köstler H, Hahn D, Beer M: Novel applications for diffusion-weighted MRI in paediatric rheumatology: imaging of bone marrow oedema, soft tissue oedema and synovitis. Pediatr Rheumatol Online J. 2012 Jul 31; 10(1): 20. DOI: 10.1186/1546-0096-10-20.
29. Gawande RS, Gonzalez G, Messing S, Khurana A, Daldrup-Link HE. Role of diffusion-weighted imaging in differentiating benign and malignant pediatric abdominal tumors. Pediatr Radiol. 2013 Jul; 43(7): 836-45. DOI: 10.1007/s00247-013-2626-0.
30. Neubauer H, Pabst T, Dick A, Machann W, Evangelista L, Wirth C, et al. Small-bowel MRI in children and young adults with Crohn disease: retrospective head-to-head comparison of contrast-enhanced and diffusion-weighted MRI. Pediatric Radiology. 2013 Jan; 43(1): 103-14. DOI: 10.1007/s00247-012-2492-1.
31. Koh DM, Collins DJ, Orton MR. Intravoxel Incoherent Motion in Body Diffusion-Weighted MRI: Reality and Challenges. AJR Am J Roentgenol. 2011 Jun; 196(6): 1351-61. DOI: 10.2214/AJR.10.5515.
32. Chandarana H, Kang SK, Wong S, Rusinek H, Zhang JL, Arizono S, et al. Diffusion-weighted intravoxel incoherent motion imaging of renal tumors with histopathologic correlation. Invest Radiol. 2012 Dec; 47(12): 688-96. DOI: 10.1097/RLI.0b013e31826a0a49.
33. Pentang G, Lanzman RS, Heusch P, Müller-Lutz A, Blondin D, Antoch G, Wittsack HJ. Diffusion kurtosis imaging of the human kidney: a feasibility study. Magn Reson Imaging. 2014 Jun; 32(5): 413-20. DOI: 10.1016/j.mri.2014.01.006.
34. Huang Y, Chen X, Zhang Z, Yan L, Pan D, Liang

C, Liu Z. MRI quantification of non-Gaussian water diffusion in normal human kidney: a diffusional kurtosis imaging study. NMR Biomed. 2015 Feb; 28(2): 154-61. doi: 10.1002/nbm.3235.

35. Panagiotaki E, Walker-Samuel S, Siow B, Johnson SP, Rajkumar V, Pedley RB, et al. Noninvasive quantification of solid tumor microstructure using VERDICT MRI. Cancer Res. 2014 Apr 1; 74(7): 1902-12. DOI: 10.1158/0008-5472.CAN-13-2511.
36. Bley TA, Wieben O, Uhl M. Diffusion-weighted MR imaging in musculoskeletal radiology: applications in trauma, tumors, and inflammation. Magn Reson Imaging Clin N Am. 2009 May; 17(2): 263-275. DOI: 10.1016/j.mric.2009.01.005.
37. Kirchner J, Gadek D, Goltz JP, Doroch-Gadek A, Stückradt S, Liermann D, Kickuth R. Standard versus inverted digital luminescence radiography in detecting pulmonary nodules: a ROC analysis. Eur J Radiol. 2013 Oct; 82(10): 1799-803. DOI: 10.1016/j.ejrad.2013.05.001.